



Discover Generics

Cost-Effective CT & MRI Contrast Agents

 **FRESENIUS
KABI**

[WATCH VIDEO](#)

AJNR

MR imaging of malignant uveal melanoma: role of pulse sequence and contrast agent.

F Mihara, K L Gupta, S Murayama, N Lee, J B Bond and B G Haik

AJNR Am J Neuroradiol 1991, 12 (5) 991-996
<http://www.ajnr.org/content/12/5/991>

This information is current as of June 5, 2025.

MR Imaging of Malignant Uveal Melanoma: Role of Pulse Sequence and Contrast Agent

Futoshi Mihara¹
 Kundan L. Gupta¹
 Sadayuki Murayama^{1, 2}
 Nam Lee^{3, 4}
 J. Brent Bond⁵
 Barrett G. Haik⁵

To determine the most sensitive pulse sequence and to clarify the role of each pulse sequence in the MR diagnosis of uveal malignant melanoma, noncontrast T1- and T2-weighted, and postcontrast T1-weighted, spin-echo images were compared blindly and independently by two experienced observers. Thirty uveal malignant melanomas, preselected by ophthalmoscopy and sonography for size greater than 2 mm, were examined with a 1.5-T superconducting MR unit with an orbital surface coil. Fifteen tumor studies were done after the patient was injected with gadopentetate dimeglumine. Postcontrast T1-weighted images were the most sensitive in detecting melanomas, demonstrating tumors 2 mm in height accurately on axial planes and 1.6 mm in height on combined orthogonal planes. The contrast-to-noise ratio between melanoma and vitreous fluid was greatest on postcontrast T1-weighted images (average, 72.1), followed by noncontrast T1-weighted images (average, 32.9), and then by T2-weighted images (average, -21.2). Postcontrast T1-weighted images also proved useful in differentiating melanomas from subretinal fluid collections when combined with noncontrast images.

We conclude that postcontrast T1-weighted images are most helpful in detecting small uveal melanomas and in differentiating melanomas from subretinal fluid collections.

AJNR 12:991-996, September/October 1991; *AJR* 157: November 1991

Received August 22, 1990; revision requested December 5, 1990; revision received February 20, 1991; accepted April 21, 1991.

Presented at the annual meeting of the American Society of Neuroradiology, Los Angeles, March 1990.

This work was supported in part by the St. Giles Foundation, Brooklyn, NY, and by an unrestricted grant from Research to Prevent Blindness, New York, NY.

¹ Department of Diagnostic Radiology, University of Maryland Medical System, 22 So. Greene St., Baltimore, MD 21201. Address reprint requests to F. Mihara.

² Present address: Department of Radiology, Faculty of Medicine, Kyushu University, Fukuoka 812, Japan.

³ Tulane University Medical Center, New Orleans, LA 70112.

⁴ Present address: Department of Radiology, University of Florida Health Science Center, Jacksonville, FL 32209.

⁵ Department of Ophthalmology, Tulane University Medical Center, New Orleans, LA 70112.

0195-6108/91/1205-0991

© American Society of Neuroradiology

Malignant uveal melanoma is the most common ocular tumor in adults [1]. Diagnosis is confirmed by ophthalmoscopy [1, 2], fluorescein angiography [1], sonography [1-4], and CT [2-4]. Although accuracy of clinical diagnosis is high [5], misdiagnoses occur occasionally [6-9]. Recent studies have shown MR to be useful in evaluating uveal melanoma [4, 10] and to be facilitated by the use of a higher magnetic field strength and surface coils [11-14]. Peyster et al. [14] compared MR and CT in the evaluation of intraocular tumors and concluded that MR is superior in both detection and differential diagnosis. Mafee et al. [13] also showed superiority of MR over CT and demonstrated that sonography may be more accurate in detecting small tumors. However, these studies only used unenhanced MR imaging.

To further assess the potential of MR imaging and to determine the value of different pulse sequences in the detection and characterization of uveal melanoma, this study evaluated precontrast T1- and T2-weighted spin-echo (SE) MR images and postcontrast T1-weighted SE images using a surface coil at 1.5 T.

Materials and Methods

Thirty patients with malignant uveal melanoma were preselected to include only patients with tumors greater than 2 mm in size as determined by ophthalmoscopy and sonography (Tables 1 and 2). Twenty-nine tumors were melanotic and one was amelanotic by ophthalmoscopy. A 1.5-T superconducting MR unit (Sigma, General Electric, Milwaukee, WI) with a 12.5-cm-diameter receive-only surface coil (General Electric, Milwaukee, WI) was used for all

TABLE 1: Uveal Melanoma on Unenhanced MR Images

Case No.	Sex	Age (yr)	Location	Size ^a (mm)	Tumor Detection		Comments
					T1-Weighted	T2-Weighted	
1	F	75	OD/P	2 × 3	+	-	
2	M	76	OS/P	2 × 6	+	+	
3	M	64	OD/PM	2 × 7	+	+	
4	F	56	OD/P	2 × 10	+	+	
5	F	41	OS/P	4 × 6	+	+	SF
6	F	64	OD/P	4 × 10	+	+	
7	M	76	OD/PM	6 × 10	+	+	
8	F	58	OS/PM	8 × 8	+	+	SF ^b
9	M	66	OD/PL	8 × 12	+	+	SF ^b
10	M	79	OD/P	9 × 10	+	+	SF ^b
11	M	35	OD/AL	10 × 10	+	+	
12	F	80	OD/L	10 × 14	+	+	SF ^b
13	M	65	OD/AM	12 × 18	+	+	SF
14	F	66	OS/P	12 × 24	+	+	
15	F	72	OD/L	14 × 18	+	+	SF ^b

Note.—+ = detected; - = not detected; OD = right eye; OS = left eye; A = anterior; P = posterior; M = medial; L = lateral; SF = subretinal fluid collection.

^a Height × base diameter.

^b Detected by MR.

cases. T1-weighted images were obtained with sequences of 500,600/20,30/2 (TR/TE/excitations); T2-weighted images were obtained with 2000/70/2. Examination planes for T1-weighted images were axial, coronal, and oblique sagittal; for T2-weighted images, only the axial plane was used. Imaging parameters were 256 × 128 matrix, 18-cm field of view, 3-mm slice thickness, and 1.5-mm slice gap. In 15 studies, 0.1 mmol/kg of gadopentetate dimeglumine (Magnevist, Berlex, Cedar Knolls, NJ) was administered.

Tumor detection rate was compared among unenhanced T1- and T2-weighted axial images, and postcontrast T1-weighted SE images. Image evaluation was performed blindly and independently by two experienced neuroradiologists. Tumors not identified by both radiologists were considered to be undetected.

In the 15 cases in which gadopentetate dimeglumine was administered, signal intensity (SI) [15] of both tumor and vitreous fluid and standard deviations (SD) of noise were obtained by region-of-interest (ROI) calculations on the image that showed maximal tumor size. Measurements from two areas of tumor and vitreous fluid and four areas of noise were averaged. Contrast-to-noise ratios (CNR) were calculated by the formula [16]

$$\text{CNR} = (\text{SI of tumor} - \text{SI of vitreous fluid}) / \text{SD of noise.} \quad (1)$$

Subretinal fluid collection associated with tumor was also evaluated in regard to gadopentetate dimeglumine enhancement, which provided further information. MR findings were correlated with sonographic findings.

Results

Melanotic melanomas showed a characteristic pattern of contrast enhancement and of signal hyperintensity on T1-weighted images and signal hypointensity on T2-weighted images relative to the signal of vitreous fluid (Fig. 1). One small amelanotic melanoma showed slight hyperintensity relative to vitreous fluid on T1-weighted images, which was not detected on T2-weighted images. All cases in which contrast material was administered showed increased tumor SI compared with noncontrast T1-weighted images.

Tumor detection is summarized in Tables 1 and 2. Of the total number of 30 uveal melanomas, T1-weighted imaging detected 27, whereas T2-weighted imaging detected 22. Of the 15 cases in which gadopentetate dimeglumine was administered, postcontrast T1-weighted imaging detected 14

cases, noncontrast T1-weighted imaging detected 12 cases, and T2-weighted imaging detected eight cases. Tumor height of 2 mm was the lower limit for accurate detection on non-contrast images, and 1.6 mm was the lower limit on postcontrast images. Small discoid melanomas were detected in two patients only on postcontrast T1-weighted images owing to tumor enhancement (Figs. 2 and 3). One tumor was not evident on any of the axial images; however, it was easily detected on both coronal and sagittal postcontrast T1-weighted images (Fig. 4).

CNR on postcontrast T1-weighted images (average, 72.1) was greater than on either noncontrast T1-weighted images (average, 32.9, *p* < .01) or T2-weighted images (average, -21.2, *p* < .001) (Table 2).

By sonography, 13 patients had subretinal fluid collections associated with tumor. These were identified in 10 cases by a combination of T1- and T2-weighted MR imaging, while three small subretinal fluid collections could not be detected on MR images. Six of the 10 patients with subretinal fluid collections seen on MR images were studied with contrast-enhanced imaging. In three of these cases the fluid collections were apparent on noncontrast images and in two cases they were equivocal; one small subretinal fluid collection could not be detected on either pre- or postcontrast images. In the two equivocal cases, the subretinal fluid collections were clearly demonstrated on postcontrast images. One subretinal fluid collection was almost isointense with vitreous fluid on both T1- and T2-weighted images. This was apparent on postcontrast images because of marked retinal or choroidal enhancement (Fig. 5). Another subretinal fluid collection was isointense with tumor on noncontrast T1-weighted images with equivocal findings on T2-weighted images, but postcontrast T1-weighted images clearly separated tumor from fluid because of tumor enhancement (Fig. 6).

Discussion

Accurate and early diagnosis of choroidal melanoma by any means is important because of the direct correlation between tumor size and mortality. Shammas and Blodi [17] reviewed a series of 293 cases of choroidal melanoma and found that tumor diameter was the single most important prognostic factor.

Tumor size not only influences prognosis but may also determine subsequent management. Newer treatment methods, such as radioactive plaque therapy, proton beam irradiation, and en bloc resection, now offer an alternative to enucleation. However, successful implementation of therapy is dependent on early identification and complete delineation.

Although MR imaging is superior to CT in the detection and differentiation of most melanomas [4, 14], neither CT nor unenhanced MR imaging has been accurate in detecting tumors smaller than 2–3 mm in height [3, 13]. Although CT is faster than MR, it adds the risk of IV administration of iodinated contrast material [3, 4] and radiation exposure to the lens [18]. Increased SI after injection of gadopentetate dimeglumine facilitates accurate detection of small tumors on MR images by offsetting partial volume averaging and providing bright signal on T1-weighted images.

Gadopentetate dimeglumine shortens both T1 and T2 relaxation times in tissue, which results in contrast enhancement on T1-weighted images [19–22]. The paramagnetic

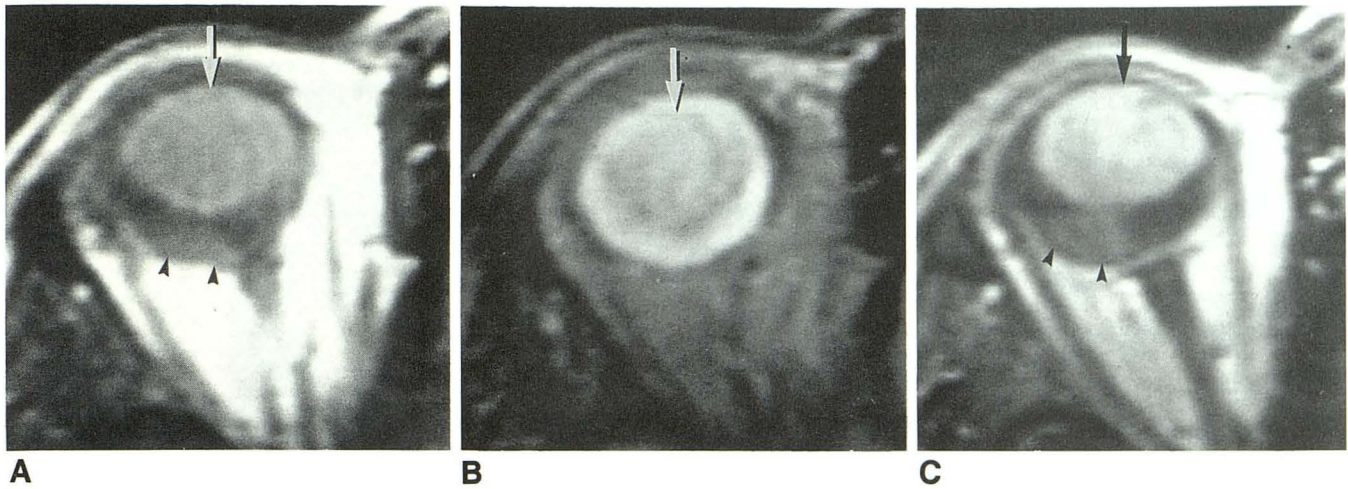


Fig. 1.—Choroidal melanoma with subretinal fluid collection.
A, Axial noncontrast T1-weighted spin-echo MR image. Tumor (*arrow*) demonstrated hyperintensity relative to vitreous fluid. Subretinal fluid (*arrowheads*) demonstrated slight hyperintensity.
B, Axial noncontrast T2-weighted spin-echo MR image. Tumor (*arrow*) demonstrated hypointensity relative to vitreous fluid. Subretinal fluid demonstrated isointensity.
C, Axial postcontrast T1-weighted spin-echo MR image. Tumor (*arrow*) demonstrated increased signal intensity whereas subretinal fluid (*arrowheads*) did not show enhancement.

TABLE 2: Uveal Melanoma on Contrast-Enhanced MR Images

Case No.	Sex	Age (yr)	Location	Size ^a (mm)	Tumor Detection/CNR			Comments
					Precontrast		Postcontrast	
					T1-Weighted	T2-Weighted	T1-Weighted	
1	M	62	OD/I	1.6 × 2.1	-/-3.1	-/-2.7	-/35.6	
2	M	69	OD/P	1.6 × 6.5	-/15.0	-/-29.3	+/18.4	
3	F	77	OD/PL	2.0 × 8.0	-/7.5	-/-15.0	+/156.9	
4	F	50	OS/A	2.0 × 9.4	+/44.8	-/-5.6	+/148.0	
5	M	82	OD/PL	2.0 × 10.4	+/10.0	-/-12.7	+/33.0	
6	F	25	OD/P	2.1 × 7.8	+/23.3	-/-35.6	+/54.1	
7	M	71	OS/P	2.5 × 8.2	+/41.0	+/-20.5	+/55.5	
8	F	81	OS/PM	3.5 × 7.0	+/51.5	+/-12.7	+/92.1	SF
9	F	36	OS/AL	6.1 × 7.5	+/54.4	-/-6.9	+/89.5	
10	F	50	OD/AL	7.5 × 11.5	+/40.0	+/-21.0	+/41.6	
11	F	43	OD/AL	9.0 × 12.0	+/25.0	+/-37.1	+/73.5	SF ^b
12	M	60	OS/P	11.6 × 14.9	+/15.3	+/-66.7	+/60.0	SF ^b
13	F	78	OD/PM	12.7 × 16.9	+/38.7	+/-31.7	+/65.8	SF ^b
14	M	33	OD/PS	13.4 × 18.3	+/60.8	+/-12.6	+/90.8	SF ^b
15	F	72	OS/PL	13.4 × 15.6	+/62.7	+/-8.2	+/67.3	SF ^b

Note.—CNR = contrast-to-noise ratio; + = detected; - = not detected; OD = right eye; OS = left eye; A = anterior; P = posterior; M = medial; L = lateral; S = superior; I = inferior; SF = subretinal fluid collection.

^a Height × base diameter.

^b Detected by MR.

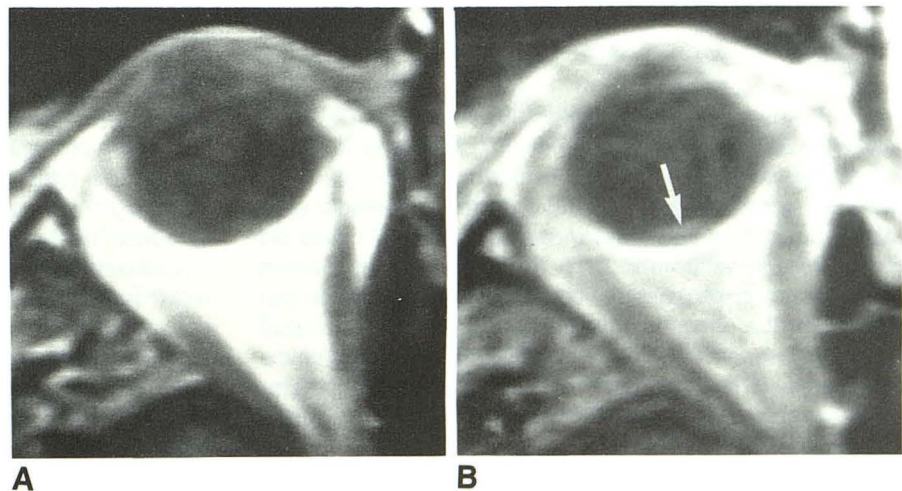


Fig. 2.—**A,** Axial noncontrast T1-weighted spin-echo MR image did not detect the lesion accurately.

B, Axial postcontrast T1-weighted spin-echo MR image detected discoid choroidal melanoma (*arrow*). Tumor size was 1.6 × 6.5 mm.

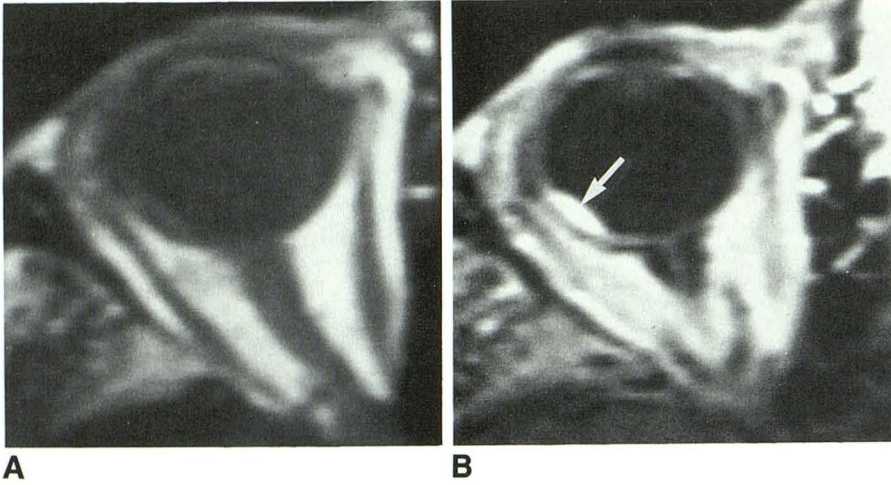


Fig. 3.—A, Axial noncontrast T1-weighted spin-echo MR image did not detect the lesion accurately.
B, Axial postcontrast T1-weighted spin-echo MR image detected discoid choroidal melanoma (arrow). Tumor size was 2.0 × 8.0 mm.

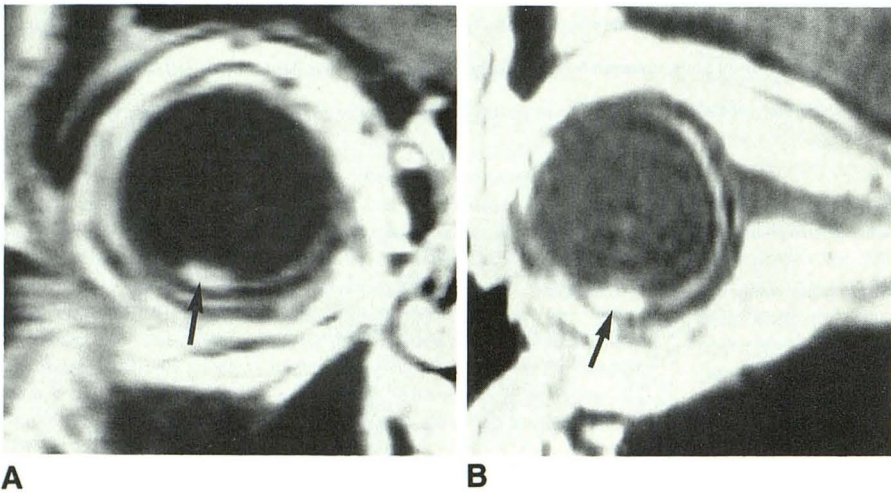


Fig. 4.—A and B, Coronal (A) and sagittal (B) postcontrast T1-weighted spin-echo MR images detected enhanced tumor (arrows) clearly.

effect seen with melanoma also decreases T1 relaxation time [4, 10, 13, 23, 24], which leads to increased SI on T1-weighted images.

Gomori et al. [24] measured the T1 and T2 relaxation times of uveal melanoma using nuclear MR spectroscopy. Moderately pigmented melanomas had average T1 and T2 relaxation times of 596 msec and 68 msec, respectively.

The observed relaxation times after administration of paramagnetic contrast agent are calculated by the formula [19, 21]

$$1/T_{\text{obs}} = 1/T_0 + R \times [C], \quad (2)$$

where T_{obs} is the measured relaxation time (sec), T_0 is T1 relaxation time (sec) of material without the contrast agent, R is the relaxivity, and $[C]$ is the concentration of paramagnetic contrast material (mmol/l). If the R of gadopentetate dimeglumine is $5 \text{ mmol}^{-1}\text{s}^{-1}$ [19], the observed T1 and T2 relaxation times are 457 msec and 65.7 msec at a gadopentetate dimeglumine concentration of 0.1 mmol/l, and 239 msec and 58.1 msec at a gadopentetate dimeglumine concentration of 0.5 mmol/l, respectively. These gadopentetate dimeglumine concentrations are theoretically calculated for enhancement on T1-weighted SE images after a routine dose of 0.1 mmol/kg [20–22].

The SI of tissues in SE imaging when $TR \gg TE$ is calcu-

lated by the formula [25]

$$SI = k \times N(H) (e^{-TE/T_2}) (1 - e^{-TR/T_1}), \quad (3)$$

where k is a constant expressing system gain, $N(H)$ is the mobile proton density, and T_1 and T_2 are relaxation times.

On the basis of the foregoing formulas and assumptions, noncontrast T1-weighted (500/20) SE images of moderately pigmented tumors show a relative SI of 0.426, 0.491 at 0.1 mmol/l of gadopentetate dimeglumine concentration and 0.621 at 0.5 mmol/l of gadopentetate dimeglumine concentration. Therefore, moderately pigmented melanoma shows increased signal after gadopentetate dimeglumine administration. It may be possible that a markedly pigmented melanoma does not increase in SI after contrast administration because shortening of the T2 relaxation time may cancel the effect of a short T1 relaxation time. However, with very short T1, highly pigmented tumors should show markedly high intensity on noncontrast T1-weighted images, facilitating detection.

T2-weighted images were least effective in detecting uveal melanoma owing to (1) low signal-to-noise ratio [13], (2) low contrast between tumor and vitreous fluid, (3) low spatial resolution [13], and (4) sensitivity to motion because of prolonged examination time [26]. This pulse sequence is better used to characterize lesions as to melanoma or other tumor, or to demonstrate subretinal fluid collection or hemorrhage.

In this study, all tumors detected by sonography were

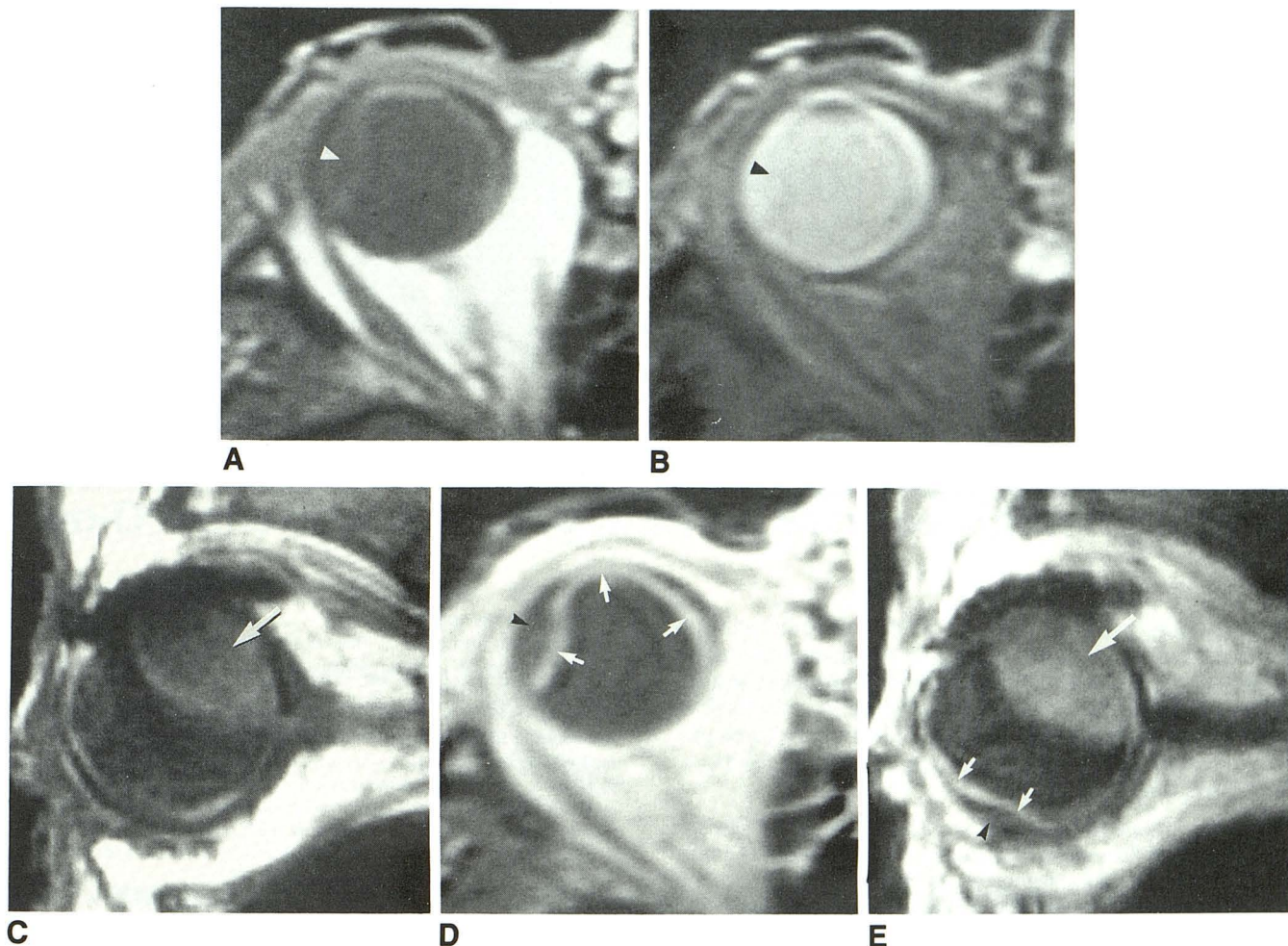


Fig. 5.—Choroidal melanoma with sudden deterioration of right-sided vision.
A and B, Axial noncontrast T1-weighted (**A**) and T2-weighted (**B**) spin-echo MR images demonstrated subretinal fluid (*arrowheads*) almost isointense with vitreous fluid.
C, Sagittal noncontrast T1-weighted spin-echo MR image demonstrated a large choroidal melanoma in posterosuperior portion of right globe (*arrow*).
D and E, Postcontrast axial (**D**) and sagittal (**E**) T1-weighted spin-echo MR images clearly delineated subretinal fluid (*arrowheads*) because of retinal or choroidal enhancement (*short arrows*). A large choroidal melanoma demonstrated appreciable enhancement (*long arrow* in **E**).

demonstrated on postcontrast T1-weighted images when orthogonal examination planes were used. Therefore, postcontrast T1-weighted images were as sensitive as sonography in demonstrating melanomas more than 1.6 mm in height. However, one small subretinal fluid collection adjacent to a small melanoma was not detected even on postcontrast MR images. Therefore, detection of such small lesions may still require a combination of imaging techniques. However, sonography is not ideal for detecting lesions of the ciliary body or for patients with painful eyes, and it increases the risk of inflammation [3]. Ophthalmoscopy may be limited in cases of opaque ocular media, vitreous hemorrhage, or large amounts of subretinal effusion [27]. In these cases, MR examination becomes even more valuable.

In this study, all MR examinations were performed with a slice thickness of 3 mm and slice gap of 1.5 mm. Reduction in slice thickness and gap is probably advantageous for detecting small tumors [12], but this can be questioned since the CNR decreases as spatial resolution increases [28, 29].

Use of a smaller matrix (i.e., 192 or 256) may help to detect small lesions because of increased spatial resolution; however, this effect will be somewhat limited by decreased CNR and increased examination time [28]. Chemical shift techniques combined with contrast enhancement may also improve detection. However, small melanomas are usually confined to the globe [17]. Consequently, they are surrounded by vitreous fluid anteriorly and demarcated by sclera posteriorly. Both structures are hypointense on T1-weighted images in contrast to melanoma. Therefore, fat suppression would not be extremely helpful in detecting small intraocular melanomas. Furthermore, use of the fat-suppression technique has the additional disadvantages of decreased signal intensity and increased artifacts [30].

In conclusion, postcontrast T1-weighted images were most sensitive in detecting uveal melanoma by MR examination. This pulse sequence was helpful in differentiating tumor from subretinal fluid collection when combined with noncontrast T1-weighted images. Findings from contrast-enhanced MR

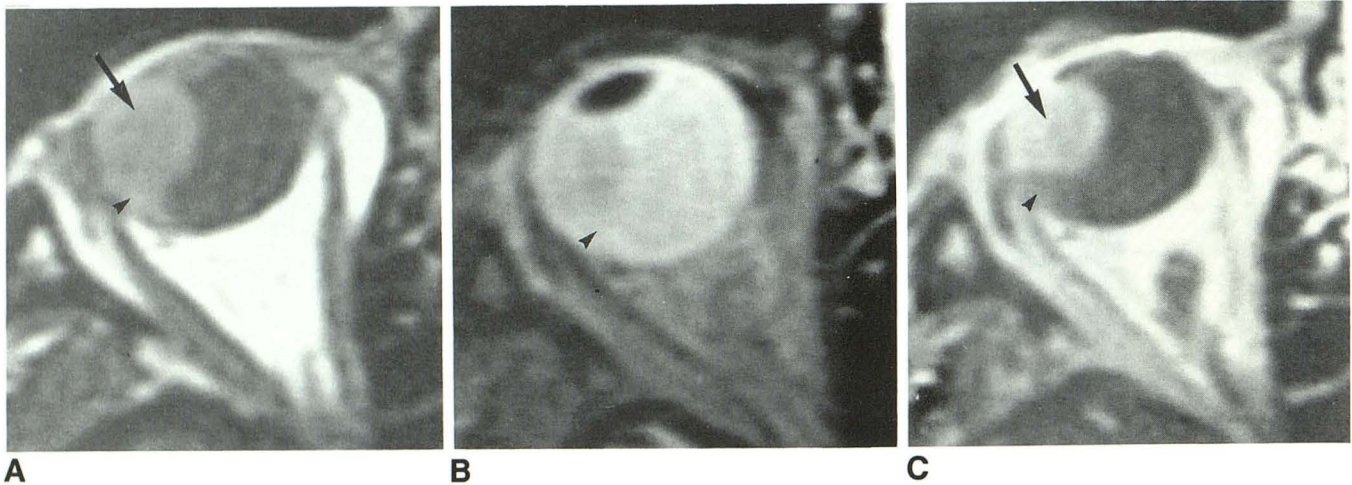


Fig. 6.—A, Axial noncontrast T1-weighted spin-echo MR image. Choroidal melanoma (arrow) and subretinal fluid collection (arrowhead) could not be clearly separated.

B, Axial noncontrast T2-weighted spin-echo MR image demonstrated equivocal findings of subretinal fluid collection (arrowhead).

C, Axial postcontrast T1-weighted spin-echo MR image separated tumor tissue (arrow) from subretinal fluid (arrowhead) because the former showed enhancement.

imaging, added to clinical data and results from other imaging techniques, provide further diagnostic information and allow confirmative diagnosis, thereby obviating unnecessary interventional procedures.

ACKNOWLEDGMENTS

We acknowledge the invaluable assistance of Arvin E. Robinson in preparing this manuscript, the patience and technical skill of Morris Francis, the professional photographs taken by Richard Hutton, and the secretarial assistance provided by Terry McGuckin.

REFERENCES

1. Shields JA. Current approaches to the diagnosis and management of choroidal melanomas. *Surv Ophthalmol* 1977;21:443-463
2. Peyster RG, Augsburger JJ, Shields JA, et al. Choroidal melanoma: comparison of CT, funduscopy, and US. *Radiology* 1985;156:675-680
3. Mafee MF, Peyman GA, McKusick MA. Malignant uveal melanoma and similar lesions studied by computed tomography. *Radiology* 1985;156:403-408
4. Mafee MF, Peyman GA, Grisolano JE, et al. Malignant uveal melanoma and simulating lesions: MR imaging evaluation. *Radiology* 1986;160:773-780
5. Char DH, Stone RD, Irvine AR, et al. Diagnostic modalities in choroidal melanoma. *Am J Ophthalmol* 1980;89:223-230
6. Roness B, Zimmerman LE. An unusual choroidal hemorrhage simulating malignant melanoma. *Arch Ophthalmol* 1963;70:30-32
7. Ferry AP. Lesions mistaken for malignant melanoma of the posterior uvea: a clinicopathologic analysis of 100 cases with ophthalmoscopically visible lesions. *Arch Ophthalmol* 1964;72:463-469
8. Shields JA. Lesions simulating malignant melanoma of the posterior uvea. *Arch Ophthalmol* 1973;89:466-471
9. Mauriello JA Jr, Zimmerman LE, Rothstein TB. Intrachoroidal hemorrhage mistaken for malignant melanoma. *Ann Ophthalmol* 1983;15:282-284
10. Haik BG, Louis ST, Smith ME, Ellsworth RM, Deck M, Friedlander M. Magnetic resonance imaging in choroidal tumors. *Ann Ophthalmol* 1987;19:218-238
11. Bilaniuk LT, Schenck JF, Zimmerman RA, et al. Ocular and orbital lesions: surface coil MR imaging. *Radiology* 1985;156:669-674
12. Sullivan JA, Harms SE. Surface-coil MR imaging of orbital neoplasms. *AJNR* 1986;7:29-34
13. Mafee MF, Peyman GA, Peace JH, Cohen SB, Mitchell MW. Magnetic resonance imaging in the evaluation and differentiation of uveal melanoma.

Ophthalmology 1987;94:341-348

14. Peyster RG, Ausberger JJ, Shields JA, Hershey BL, Eagle R Jr, Haskin ME. Intraocular tumors: evaluation with MR imaging. *Radiology* 1988;168:773-779
15. Enzmann DR, O'Donohue J. Optimizing MR imaging for detecting small tumors in the cerebellopontine angle and internal auditory canal. *AJNR* 1987;8:99-106
16. Mano I, Yoshida H, Nakabayashi K, Yashiro N, Iio M. Fast spin echo imaging with suspended respiration: gadolinium enhanced MR imaging of liver tumors. *J Comput Assist Tomogr* 1987;11:73-80
17. Shamma HF, Blodi FC. Prognostic factors in choroidal and ciliary body melanomas. *Arch Ophthalmol* 1977;95:63-69
18. Mafee MF, Linder B, Peyman GA, Langer BG, Choi KH, Capek V. Choroidal hematoma and effusion: evaluation with MR imaging. *Radiology* 1988;168:781-786
19. Weinmann HJ, Brasch RC, Press WR, Wesbey GE. Characteristics of gadolinium-DTPA complex: a potential NMR contrast agent. *AJR* 1984;142:619-624
20. Weinmann HJ, Laniado M, Mutzel W. Pharmacokinetics of GdDTPA/dimeglumine after intravenous injection into healthy volunteers. *Physiol Chem Phys Med NMR* 1984;16:167-172
21. Weinmann HJ, Gries H, Speck U. Gd DTPA and low osmolar Gd chelates. In: Runge VM, ed. *Enhanced magnetic resonance imaging*. St. Louis: Mosby, 1989:74-86
22. Elster AD, Sobol WT, Hinson WH. Pseudolayering of Gd-DTPA in the urinary bladder. *Radiology* 1990;174:379-381
23. Damadian R, Zaner K, Hor D. Human tumors by NMR. *Physiol Chem Phys* 1973;5:381-402
24. Gomori JM, Grossman RI, Shields JA, Augsburger JJ, Joseph PM, DeSimeone D. Choroidal melanomas: correlation of NMR spectroscopy and MR imaging. *Radiology* 1986;158:443-445
25. Hendrick RE, Newman FD, Hendee WR. MR imaging technology: maximizing the signal-to-noise ratio from a single tissue. *Radiology* 1985;156:749-752
26. Atlas AW, Grossman RI, Axel L, et al. Orbital lesions: proton spectroscopic phase-dependent contrast MR imaging. *Radiology* 1987;164:510-514
27. Peyman GA, Mafee MF. Uveal melanoma and similar lesions: the role of magnetic resonance imaging and computed tomography. *Radiol Clin North Am* 1987;25:471-486
28. Wehrli FW, Kanal E. Orbital imaging: factors determining magnetic resonance imaging appearance. *Radiol Clin North Am* 1987;25:419-427
29. Kucharczyk W, Crawley AP, Kelly WM, Henkelman RM. Effect of multislice interference on image contrast in T2- and T1-weighted MR images. *AJNR* 1988;9:443-451
30. Hendrix LE, Kneeland JB, Houghton VM, et al. MR imaging of optic nerve lesions: value of gadopentetate dimeglumine and fat-suppression technique. *AJNR* 1990;11:749-754